Nuclear Instruments and Methods in Physics Research B 272 (2012) 426–429

Contents lists available at ScienceDirect

Nuclear Instruments and Methods in Physics Research B

journal homepage: www.elsevier.com/locate/nimb

Damage accumulation and annealing behavior in high fluence implanted MgZnO

A.Yu. Azarov [a,*], A. Hallén [b], B.G. Svensson [a], X.L. Du [c], A.Yu. Kuznetsov [a]

[a] Department of Physics, University of Oslo, P.O. Box 1048 Blindern, NO-0316 Oslo, Norway
[b] ICT-MAP, Royal Institute of Technology, Electrum 229 SE-164 40, Kista-Stockholm, Sweden
[c] Institute of Physics, The Chinese Academy of Sciences, Beijing 100190, China

ARTICLE INFO

Article history:
Available online 1 February 2011

Keywords:
Ion implantation
Damage
Annealing
MgZnO

ABSTRACT

Molecular beam epitaxy grown $Mg_xZn_{1-x}O$ ($x \leqslant 0.3$) layers were implanted at room temperature with 150 keV $^{166}Er^+$ ions in a fluence range of 5×10^{15}–3×10^{16} cm^{-2}. Evolution of ion-induced damage and structural changes were studied by a combination of Rutherford backscattering spectrometry, nuclear reaction analysis and time-of-flight elastic recoil detection analysis. Results show that damage production enhances in both Zn- and O-sublattices with increasing the Mg content in the MgZnO. However, MgZnO as well as pure ZnO exhibits a high degree of dynamic annealing and MgZnO can not be amorphized even at the highest ion fluence used. Annealing of heavily damaged ZnO leads to a strong surface erosion and thinning of the film. Increasing the Mg content suppresses the surface evaporation in high fluence implanted MgZnO but leads to a strong surface decomposition accompanied with a Mg-rich surface layer formation during post-implantation annealing.

1. Introduction

Zinc oxide (ZnO) is a direct band-gap semiconductor with numerous promising applications in optoelectronics [1,2] due to the wide band gap ($E_g \approx 3.4$ eV) and large exciton binding energy (~60 meV) at room temperature. Band-gap engineering is one of the key issues for the formation of heterostructures and quantum wells, which are needed for fabrication of modern devices. Alloying of wurtzite ZnO with rock salt MgO ($E_g \approx 7.8$ eV) [3] provides a possibility to increase the band gap. However, the fabrication of wurtzite MgZnO is challenged by phase separation occurring at high Mg contents [4].

Ion implantation is a very attractive technological tool in semiconductor processing and it can be used to introduce controllable impurity concentrations at a precise depth below the surface. It has been shown that ZnO has an extremely strong degree of dynamic annealing even at low irradiation temperatures [5,6]. However, these processes are not perfect and various types of defects are accumulated in the material during the ion bombardment [5,7]. Therefore, post-implantation annealing is needed to remove the ion-beam-induced damage. It has been shown that the effective recovery of implantation defects needs high temperatures, often in excess of 1000 °C [8,9]. Furthermore, annealing of ion-induced damage is affected by the nature of the implanted ions [8] and is further complicated by possible surface decomposition [10]. Another major issue is the dopant redistribution during ion implantation and subsequent annealing in ZnO. For example, it has been shown that the final concentration profiles of implanted rare earth elements, such as Tb [11], Er [12] and Tm [13], may be far from that predicted theoretically due to a dramatic redistribution of implanted atoms toward the surface during an annealing.

Despite intensive studies of ion-beam related phenomena in ZnO during the last decade [5–9,11–14], the understanding of radiation damage formation and annealing mechanisms in this material is still immature. Furthermore, there is very little known about radiation damage formation in ZnO-based ternary oxides. Our initial results [15] revealed enhancing complexity of radiation damage formation in MgZnO compared to that in pure ZnO. In this work we study the effects of the Mg composition on damage accumulation, its annealing and the thermal stability of high fluence Er implanted MgZnO films.

2. Experimental

About ~1 m thick $Mg_xZn_{1-x}O$ ($x = 0.1$ and 0.3) as well as pure ZnO layers were grown by molecular beam epitaxy (MBE) on sapphire substrate. Samples were implanted with 150 keV $^{166}Er^+$ ions using an ion flux of 2.5×10^{12} cm^{-2} s^{-1} in a fluence range of 5×10^{15}–3×10^{16} cm^{-2}. The implantation was carried out at room temperature at 7° off the [0001] direction in order to minimize channeling. After the implantation samples were annealed at 700 °C for 30 min. in vacuum.

Implantation-induced disorder before and after annealing was measured by Rutherford backscattering/channeling spectrometry (RBS/C) with 2 MeV $^4He^+$ ions incident along the [0001] direction

* Corresponding author. Tel.: +47 450 62 754; fax: +47 228 56 422.
E-mail address: a.y.azarow@smn.uio.no (A.Yu. Azarov).

0168-583X/$ - see front matter © 2011 Elsevier B.V. All rights reserved.
doi:10.1016/j.nimb.2011.01.115

and backscattered into detectors at 170° and 100° relative to the incident beam direction. The 100°, so-called glancing-angle detector, geometry was used to provide enhanced depth resolution for examining the near-surface damage accumulation. In addition to the conventional RBS/C, higher energy experiments were performed to get the non-Rutherford cross section to enhance the yield from displaced oxygen atoms. For this purposes $^{16}O(\alpha,\alpha)^{16}O$ nuclear reaction analysis in channeling mode (NRA/C) [16] was carried out at the scattering angle of 170°. The resonant is centered around $E = 3.045$ MeV and has an enhanced cross section with a factor of 17 compared to the regular Rutherford cross section. All RBS/C spectra were analyzed with one of the conventional algorithms [17] for extracting the effective number of scattering centers, referred as "relative disorder" below. The relative damage in oxygen sublattice was calculated from NRA/C spectra as $(\chi_{ch}-\chi_v)/(\chi_r-\chi_v)$, where χ_{ch} and χ_v – are the maximum resonant peak values in channeling spectra for the implanted and virgin samples, respectively, while χ_r – is the corresponding random value at the same depth.

Time-of-flight elastic recoil detection analysis (ToF-ERDA), using a 40 MeV ^{127}I ion beam with a recoil angle of 45° was applied to measure the elemental depth profiles through the films. Analysis of raw recoil ToF-ERDA spectra was done using the CONTES code [18].

3. Results and discussion

3.1. Damage accumulation

Fig. 1 shows RBS/C spectra of (a) pure ZnO and (b) $Mg_{0.3}Zn_{0.7}O$ implanted at room temperature with $^{166}Er^+$ ions to different ion fluences. The peak in the RBS/C spectra for channel numbers more than 320 is related to a signal from implanted Er atoms. It is seen that in both samples the damage accumulation exhibits saturation with increasing ion fluence. It is important to note that damage level in the bulk does not reach the random level in Fig. 1 even at highest ion fluence used (3×10^{16} cm^{-2}). Thus, our results support that MgZnO, as well as ZnO, exhibit a high degree of dynamic annealing during irradiation and it can not be amorphized at room temperature by heavy ion bombardment with high fluences. For the low ion fluence (most pronounced for the lowest fluence of 5×10^{15} cm^{-2}) the disorder profiles in pure ZnO are bimodal with clearly distinguishable "bulk" and "surface" damage peaks. Interestingly, the damage accumulation in $Mg_{0.3}Zn_{0.7}O$ exhibits unimodal behavior for all ion fluences resulting in enhanced disorder in comparison to that in pure ZnO. The effect of Mg content on the damage buildup is illustrated by Fig. 1c, which compares the depth profiles of relative disorder in the Zn-sublattice as a function of Mg content in samples implanted with the same ion fluence of 5×10^{15} cm^{-2}. It is clearly seen that an increase in the Mg content strongly enhances the damage accumulation in the region between the bulk and surface damage peaks, labeled with arrows in Fig. 1c. Possible reasons for the enhanced damage production in MgZnO with increasing Mg content were recently discussed elsewhere [15] and interpreted in terms of retardation of dynamic annealing and/or effects of phase separation in the region between the bulk damage peak and the film surface. Further, the comparison of random spectra of the unimplanted and 3×10^{16} cm^{-2} implanted samples reveals the reduced Zn concentration in the near surface region which may be attributed to the Er incorporation or sputtering effects (see Fig. 1a and b).

Elemental depth profiles of $Mg_{0.3}Zn_{0.7}O$ implanted with $^{166}Er^+$ ions to a fluence of 3×10^{16} cm^{-2} are shown in Fig. 2. It is clearly seen that high fluence Er implantation leads to a depletion of the Zn concentration in the near surface region comparing to the uniform Zn profile in the virgin sample (not shown). Concurrently, O concentration increases in the same area, while the Mg

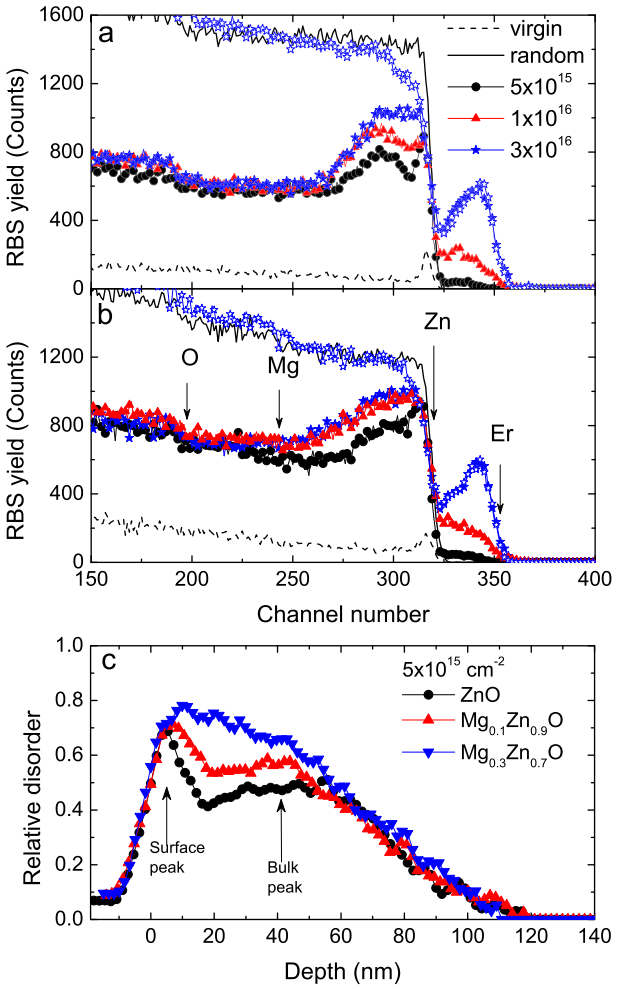

Fig. 1. Random (open symbols) and channeling (closed symbols) RBS spectra (acquired with 100° detector geometry) of (a) pure ZnO and (b) $Mg_{0.3}Zn_{0.7}O$ bombarded at room temperature by 150 keV $^{166}Er^+$ ions with different fluences as indicated in the legends. The positions of Zn, O, Mg and Er at the film surface are shown by the arrows in panel (b). The random and channeling "virgin" spectra of the unimplanted samples are shown by the solid and the dashed lines, respectively. (c) Comparison of depth profiles of relative disorder in Zn sublattice in the samples having different Mg content and implanted with the same ion fluence of 5×10^{15} cm^{-2}.

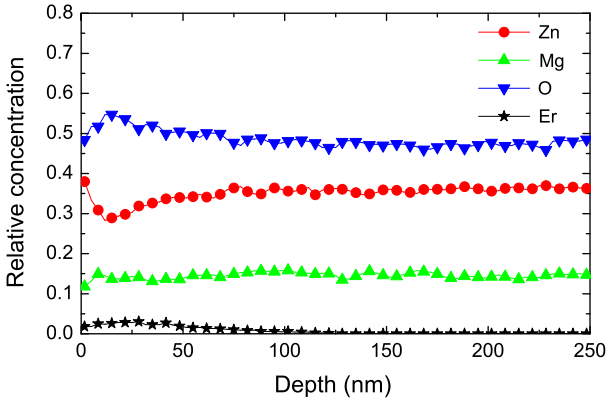

Fig. 2. The depth profiles (extracted from ToF-ERDA spectra) of relative concentration of Zn, O, Mg and Er atoms in $Mg_{0.3}Zn_{0.7}O$ bombarded at room temperature with 150 keV $^{166}Er^+$ ions to 3×10^{16} cm^{-2}.

concentration remains almost unchanged. The enhancement of the O concentration in the implanted region may by attributed to chemical effects of implanted species e.g. the Er-oxide formation. In addition, the difference in Zn and Mg profiles may indicate the preferential sputtering of Zn atoms. Thus, a significant material decomposition occurs in MgZnO as a result of high fluence Er implantation, making the near surface region enriched with O possibly due to chemical and/or preferential sputtering effects.

Note that it is not possible to draw any conclusion about damage accumulation in the oxygen sublattice due to low intensity of the oxygen peak in the conventional RBS/C spectra (see Fig. 1). In order to estimate the damage in oxygen sublattice we performed NRA/C with the incident ^{4}He beam energies close to the 3.045 MeV resonance for ^{16}O(α,α) ^{16}O nuclear reaction. Fig. 3 shows a part of NRA/C spectra of implanted $Mg_{0.3}Zn_{0.7}O$ samples as a function of the incident ^{4}He beam energies so that the resonance appears at the depth where the analyzing atoms slows down to 3.045 MeV. For clarity, the inset in Fig. 3 shows the full NRA spectrum with the resonance position indicated by the arrow. This result potentially can be used to analyze the depth profile of displaced oxygen atoms by comparing the data in channeling and random geometries. However, accurate oxygen sublattice damage profiling in MgZnO by NRA/C is challenged by overlapping of oxygen signal from the film with the signals from the both Al from sapphire substrate and Mg. It should also be noted that in the case of resonant scattering the depth resolution is limited by the width of the resonance (~70 nm for the present measurements). With all these said the 3.05 MeV spectra in Fig. 3 reflect the displaced oxygen atoms in the near surface region. The depth of ^{16}O(α,α) ^{16}O resonance for the 3.07 MeV ^{4}He beam roughly corresponds to the depth of the bulk damage peak as determined in Fig. 1. Finally, the depth of the oxygen resonance for the 3.09 MeV ^{4}He beam corresponds to the radiation damage tail at larger depth.

Fig. 4 summarizes the RBS/C and NRA/C results and shows (a) the maximum relative disorder in Zn-sublattice at the depth of the bulk peak and (b) relative damage level in O-sublattice, both in the near surface region and bulk peak areas, as a function of Mg content in MgZnO films. Also note that the depth from where the data represented by "stars" in Fig. 4, are collected may not necessarily be exactly the same in panels (a) and (b). Moreover, the algorithms used for the calculation of relative disorder from RBS/C and NRA/C data are not the same either. Therefore, a direct comparison of disorder levels for Zn- and O-sublattices shown in Fig. 4(a) and (b) have limitations. Despite that, several clear features for the damage accumulation in Fig. 4 are of interest. Firstly, in the range of the bulk peak the O-sublattice disorder exhibits a similar saturation trend with increasing Mg content as that previously discussed for Zn-sublattice [15]. Secondly, the damage level in oxygen sublattice in the near surface region in Fig. 4b almost reaches the unity for highest ion fluence indicating that all oxygen atoms are displaced in this region. It should be noted that chemical effects like Er-oxide formation may affect the apparent disorder in the near surface region in oxygen sublattice.

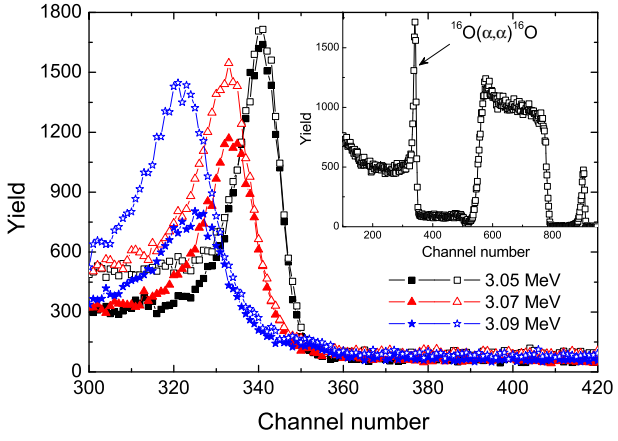

Fig. 3. Oxygen portion of the NRA spectra of the 3×10^{16} Er/cm^2 implanted $Mg_{0.3}Zn_{0.7}O$ as a function of incident ^{4}He ions energies as indicated in the legend. Open and closed symbols represent the data taken in random and channeling geometries, respectively. The full NRA spectrum and position of the ^{16}O(α,α) ^{16}O resonance are shown in the inset.

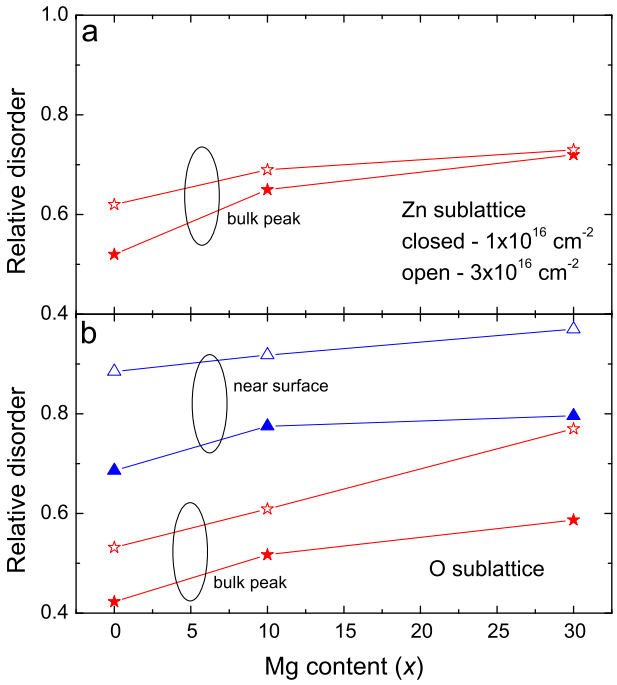

Fig. 4. (a) Maximum relative disorder in the bulk damage peak for Zn-sublattice and (b) relative damage in O-sublattice as determined by RBS/C and NRA/C analysis, respectively, as a function of Mg content in MgZnO. The samples were implanted at room temperature by 150 keV ^{166}Er$^+$ ions with ion fluences of 1×10^{16} cm^{-2} (closed symbols) and 3×10^{16} cm^{-2} (open symbols). See the text for the details.

3.2. Annealing behavior

Fig. 5 illustrates the structural evolution in (a) pure ZnO and (b) $Mg_{0.3}Zn_{0.7}O$ implanted with Er ions to the ion fluence of 3×10^{16} cm^{-2} and subjected to annealing at 700 °C for 30 min. The positions of Zn and Mg at the film surface are indicated by arrows in the panel (b). It is seen from Fig. 5a that the whole ZnO layer is accessed by RBS and after annealing the channeling spectrum becomes close to the virgin one. However, the apparent restoration of the crystallinity is attributed to a strong surface erosion and thinning of ZnO film, that is supported by the shift of the inner boundary of Zn signal toward the higher channels (from ~200 towards ~225). Interestingly, that despite the surface erosion there is no loss of Er, which is segregated at the surface. The observed strong surface erosion in ZnO at relatively low annealing temperature is consistent with previous studies of ZnO annealing. Indeed, Coleman et al. have shown that heavily damaged ZnO has a lower thermal stability compared to as-grown material and tends to decompose and evaporate during a thermal treatment [19]. Despite that these processes occur at significantly higher temperatures (>1000 °C) in ZnO, the surface erosion can be more pronounced during vacuum annealing which is used in the present study. Note that, an apparent damage recovery accompanied with dopant segregation at the sample surface reported by Rita et al. in heavy ion implanted and annealed ZnO [12,13] may be

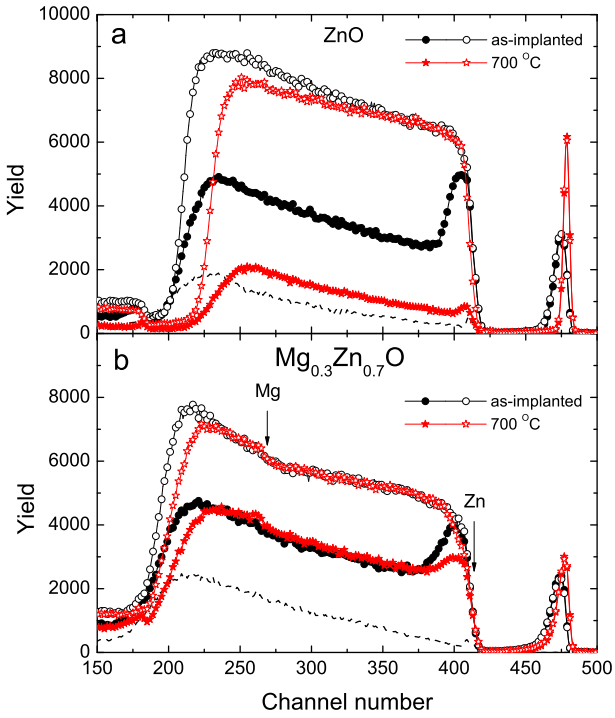

Fig. 5. The random (open symbols) and channeling (closed symbols) RBS spectra (acquired with 170° detector geometry) of (a) pure ZnO (b) $Mg_{0.3}Zn_{0.7}O$ bombarded at room temperature by 150 keV $^{166}Er^{+}$ ions to an ion fluence of 3×10^{16} cm^{-2} and subjected to annealing at 700 °C for 30 min. Virgin spectra are shown for comparison.

alternatively explained by a strong surface evaporation similar to that observed in Fig. 5a, revealing the importance of the film stability for the interpretation of RBS/C results.

The annealing behavior in MgZnO is different from that occurring in pure ZnO as illustrated by Fig. 5b. Indeed, both the surface erosion and the Er redistribution phenomena caused by the annealing are less pronounced in $Mg_{0.3}Zn_{0.7}O$ in comparison to that in pure ZnO. Furthermore, annealing has a small effect on the ion-induced damage in $Mg_{0.3}Zn_{0.7}O$. However, a decrease of the Zn signal for random spectrum and an increase of Mg signal in both channeling and random spectra in the vicinity of surface are observed. All these spectral changes indicate the film decomposition with Zn loss from the surface and a Mg-rich surface layer formation. Thus, damage annealing in MgZnO is also complicated by the low thermal stability of the film surface.

4. Conclusions

Radiation damage and annealing behavior in MgZnO implanted with Er ions to high fluences have been studied. The damage accumulation was measured in both Zn- and O-sublattices separately. The results show that overall disorder increases with increasing the Mg content in the MgZnO specifically in the region between the bulk and the surface damage peaks, but exhibits saturation consistently with previous observations. For high fluences the damage accumulation in oxygen sublattice is possibly influenced by chemical effects of Er atoms in the vicinity of the surface. Annealing at 700 °C of pure ZnO implanted with 3×10^{16} Er/cm^2 leads to the strong surface erosion and thinning of the film, while Er atoms are segregated at the surface. Increasing the Mg content suppresses the surface evaporation in high fluence implanted MgZnO but leads to a strong surface decomposition accompanied with a Mg-rich surface layer formation during post-implantation annealing.

Acknowledgements

Financial support from the Norwegian Research Council via FRINAT and RENERGI programs is acknowledged. The international cooperation was partially funded by NordForsk and Chinese Academy of Science.

References

[1] Ü. Özgür, Ya.I. Alivov, C. Liu, A. Teke, M.A. Reshchikov, S. Doğan, V. Avrutin, S.-J. Cho, H. Morkoç, J. Appl. Phys. 98 (2005) 041301.
[2] A.B. Djurišić, A.M.C. Ng, X.Y. Chen, Prog. Quantum Electron. 34 (2010) 191.
[3] T. Makino, Y. Segawa, M. Kawasaki, A. Ohtomo, R. Shiroki, K. Tamura, T. Yasuda, H. Koinuma, Appl. Phys. Lett. 78 (2001) 1237.
[4] J.L. Morrison, J. Huso, H. Hoeck, E. Casey, J. Mitchell, L. Bergman, M.G. Norton, J. Appl. Phys. 104 (2008) 123519.
[5] S.O. Kucheyev, J.S. Williams, C. Jagadish, J. Zou, C. Evans, A.J. Nelson, A.V. Hamza, Phys. Rev. B 67 (2003) 094115.
[6] C.W. White, L.A. Boatner, P.S. Sklad, C.J. McHargue, S.J. Pennycook, M.J. Aziz, G.C. Farlow, J. Rankin, Mater. Res. Soc. Symp. Proc. 74 (1987) 357.
[7] C. Ronning, P.X. Gao, Y. Ding, Z.L. Wang, D. Schwen, Appl. Phys. Lett. 84 (2004) 783.
[8] E. Sonder, R.A. Zhur, R.E. Valiga, J. Appl. Phys. 64 (1988) 1140.
[9] T. Monteiro, C. Boemare, M.J. Soares, E. Rita, E. Alves, J. Appl. Phys. 93 (2003) 8995.
[10] R. Khanna, K. Ip, Y.W. Heo, D.P. Norton, S.J. Pearton, F. Ren, Appl. Phys. Lett. 85 (2004) 3468.
[11] S. Zhou, K. Potzger, A. Mücklich, F. Eichhorn, M. Helm, W. Skorupa, J. Fassbender, Nucl. Instr. and Meth. B 266 (2008) 589.
[12] E. Rita, E. Alves, U. Wahl, J.G. Correia, T. Monteiro, M.J. Soares, A. Neves, M. Peres, Nucl. Instr. and Meth. B 242 (2006) 580.
[13] E. Rita, E. Alves, U. Wahl, J.G. Correia, A.J. Neves, M.J. Soares, T. Monteiro, Physica B 340-342 (2003) 235.
[14] K. Lorenz, E. Alves, E. Wendler, O. Bilani, W. Wesch, M. Hayes, Appl. Phys. Lett. 87 (2005) 191904.
[15] A.Yu. Azarov, B.G. Svensson, A. Hallén, X.L. Du, A.Yu. Kuznetsov, J. Appl. Phys. 108 (2010) 033509.
[16] M. Watamori, K. Oura, T. Hirao, K. Sasabe, Nucl. Instr. and Meth. B 118 (1996) 233.
[17] K. Schmid, Radiat. Eff. 17 (1973) 201.
[18] M.S. Janson, CONTES (conversion of time-energy spectra) a program for ERDA data analysis. Internal Report, Uppsala University, 2004.
[19] V.A. Coleman, H.H. Tan, C. Jagadish, S.O. Kucheyev, J. Zou, Appl. Phys. Lett. 87 (2005) 231912.